QUIET Celestial Gain Calibrations

K. Huff

May 13,2008

Polarimeter Gain Calibration Anisotropies in the polarization of the Cosmic Microwave Background have the potential to allow us to peer into the early moments of the universe and extract constraints for the cosmological constants. In order to study the CMB and its polarization, QUIET must have well calibrated polarimeters (henceforth referred to as *modules*). QUIET module calibration occurs both in the lab and in the field. In the lab, known polarized signals are created by reflecting thermal loads to the modules from rotating metal plates. In the field, celestial radio sources will provide known signals and the entire array of components, from the backplanes to the feed horns will be calibrated as as a whole. Investigation of this data will allow the multi-element array to be calibrated *a posteriori*, as an array of individual detectors with independent gain functions, leakage terms, detector axis corrections, etc. Gain calibrations in the field will be the subject of this document in which we suggest the use of TauA and CenA and discuss the pros and cons of other potential celestial calibrators.

Document Scope

- To determine what needs to be calibrated and with what precision.
- To determine which celestial radio sources to observe, explaining what makes a source ideal.
- To determine when those sources are available for observation.
- To discuss scanning strategies to observe them.
- To compile polarized flux data on these radio sources for use in data analysis later.
- To give the dependence of gain accuracy and detector angle accuracy on observation time.

1 Comparing known Source Measurements to QUIET Data

In order to derive an expected signal estimation from the published polarized fluxes of a radio source it is necessary to traverse a small forest of astronomical refrence frames and unit conversions. Much of this adventure closely follows Glen Nixon's documents[20] and Matt Hedman's document[7] detailing the TauA gain calibrations for CAPMAP, a predecessor of QUIET.

1.1 QUIET Gain

The complex gains of the QUIET apparatus can be broken down into a few distinct factors. The first is the gain from the feedhorn-OMT assembly. This assembly then feeds an A leg and a B leg signal into the module. From the appendices of Alex Sugarbaker's thesis[25], the general case of a module with unequal gains in legs A and B can be described by the four output voltages of the module. This would have complex repurcussions on gain calibration, except that these voltages will be demodulated such that Q and U can be extracted nonetheless[25].

$$V_1 = \frac{1}{8}((g_A{}^2 + g_B{}^2)I + (g_A{}^2 - g_B{}^2)V \pm 2g_A g_B Q) \longrightarrow S_1 = \frac{1}{2}g_A g_B Q \quad (1)$$

$$V_2 = \frac{1}{8}((g_A{}^2 + g_B{}^2)I + (g_A{}^2 - g_B{}^2)V \mp 2g_A g_B U) \longrightarrow S_2 = -\frac{1}{2}g_A g_B U$$

$$V_3 = \frac{1}{8}((g_A{}^2 + g_B{}^2)I + (g_A{}^2 - g_B{}^2)V \pm 2g_A g_B U) \longrightarrow S_3 = \frac{1}{2}g_A g_B U$$

$$V_4 = \frac{1}{8}((g_A{}^2 + g_B{}^2)I + (g_A{}^2 - g_B{}^2)V \mp 2g_A g_B Q) \longrightarrow S_4 = -\frac{1}{2}g_A g_B Q$$

For obvious reasons, the demodulated voltage signals, S, may later be referred to as $S_{\pm Q,\mp U}$. Perceived Q and U at the detector are functions of the QUIET optics and electronics so this document details the corrections which account for observation angles, beamsizes, etc. Once these corrections are in place we can characterize the gain of each module i as a single term, g_i which has units of mV/K.

1.2 Blackbody Conversion

Flux measurements are often reported in the detector-independent SI flux density unit of Janskys $10^{-26}Wm^{-2}Hz^{-1}$. It is important to note that the specific intensity of the source, $I(\theta,\phi)$ in Janskys per steradian ($10^{-26}Wm^{-2}Hz^{-1}sr^{-1}$) is just the flux density distribution over the source area, A.

$$F_s \;=\; \int_{source} I(\theta,\phi)dA$$

More useful for our understanding though, will be the expected QUIET signal in degrees Kelvin. In order to convert from one to the other, we use the Rayleigh-Jeans approximation to arrive at the brightness temperature over the detector area Ω_B. In terms of the flux density, F in Janskys, for the case in which the source exactly fills the detector beam area, $A = \Omega_B$, the dependence of the expected signal temperature on the detector area is not explicit in the calculation but implicit within the integration.

$$T = \frac{10^{-26}c^2}{2k_B\nu^2\Omega_B}F = \frac{F}{g_{RJ}\Omega_B} \tag{2}$$

Temperature scales inversely with the beam solid angle.

$$\Omega_B = 2\pi\sigma^2 \tag{3}$$

In QBand the HPBW is 28 arcminutes[4] and so has a solid angle of 7.517×10^{-5} steradians. So, for Q-Band at 42 GHz the expected signal is $259\mu K/Jy$. For W-Band at 90 GHz the beamwidth is 12.6 arcmin[4], which corresponds to a solid angle of 1.522×10^{-5} and a temperature of $278\mu K/Jy$. As a point of reference, the CMB, with a temperature of $3^\circ K$, has an flux density of 11.6 MJy in a Q-Band detector and 10.8 MJy in a W-Band detector. Also, WMAP has beam solid angles of 7.923×10^{-5}steradians in QBand and 1.474×10^{-5} in WBand[15]. This comparison will be used when extrapolating from WMAP reported Janskys to QUIET temperatures. Since T is inversely proportional to Ω_B we find:

$$T_{\text{QUIET}} = T_{\text{WMAP}}\frac{\Omega_{\text{WMAP}}}{\Omega_{\text{QUIET}}} \tag{4}$$

$$\left(\frac{\Omega_{\text{WMAP}}}{\Omega_{\text{QUIET}}}\right)_{\text{QBAND}} = 1.05$$

$$\left(\frac{\Omega_{\text{WMAP}}}{\Omega_{\text{QUIET}}}\right)_{\text{WBAND}} = 0.97 \tag{5}$$

Clearly these ratios are very close to 1 as expected in both cases.

1.3 Parallactic Angle Correction

By observing the same source at different positions in its path across the sky, or alternatively by rotating the detector axes in relation to the source in a smaller range of azimuthal angles, we can separate the leakage terms from the real polarization measurements. Greater accuracy is achieved with

a greater range of parallactic angle. So, in choosing calibration sources, we prefer those that traverse a large range of parallactic angles, χ, where[3]

$$\chi = \tan^{-1}\left(\frac{\cos(lat)\sin(ha)}{\sin(lat)\cos(dec) - \cos(lat)\sin(dec)\cos(ha)}\right) \tag{6}$$

Where *ha* is the source hour angle, *dec* is the source declination, and *lat* the latitude of the telescope in Chajnator, Chile ($23°1'9.48$"). As the parallactic angle changes, the source polarization axes tilt with the IAU definition of the U and Q polarization axes on the sky. Matt Hedman's thesis provides an informative graphic of the IAU definition[6], and Colin's document on the Chicago coordinate conventions contains one for the parallactic angle[2] (see appendix). Here, the parallactic angle correction relates the orthogonal Q and U components of detected polarization to the polarization of the soure, by reducing the source polarization by the correction factor:

$$\cos\left(\frac{\chi_i - (\Phi_d - \Phi_p)}{2}\right) \tag{7}$$

where χ_i is the parallactic angle from the telescope to the source during the measurement, i. Φ_d is the detector angle with respect to the vertical. Φ_p is the parallactic angle of the source polarization. So, if one of our detector axes is at Φ_{d1} then, by design, the other is at $\Phi_{d2} = \Phi_{d1} + \frac{\pi}{2}$ and we observe that, for example, a source with a polarization P in μK with an axis at Φ_p the observed signal from our two detector axes is a function of χ_i.[7]

$$P_{+Q} = \cos\left(\frac{\chi_i - (\Phi_d - \Phi_p)}{2}\right)P \tag{8}$$

With numerous parallactic angle observations, this will isolate Q to U leakage in each module signal. In order to determine the parallactic angle ranges for each potential source fromt he perspective of the telescope in Chajnantor, Chile, I accessed the IDL AstroLibrary. My resulting plots can be found in the Appendix.

1.4 Point Sources

Some radio sources of interest such as blazars are point sources, unresolvable by the QUIET beam. That is to say, for Q-Band the diameters of these sources are smaller than $0.35°$ and for W-Band they are smaller than $0.15°$. For a point source, a pixel includes the integrated signal over an area larger than the source but including the source, so we may treat it as if the source irradiance were a delta function.[20] So we may say,

$$\begin{aligned} S_{\pm Q,\mp U} &= \frac{g_A g_B}{2} A\delta\nu[I \otimes B(\theta,\phi)] \\ &= \frac{g_A g_B}{2} A\delta\nu P_{\pm Q,\mp U}[\delta(\theta,\phi)B(\theta,\phi)] \end{aligned} \tag{9}$$

where A_i is the effective area of that detector, $\delta\nu$ is the bandwidth, $I \otimes B(\theta, \phi)$ is the convolution of source irradiance function with the beam profile, and $P_{\pm Q, \mp U}$ is the source polarization in Kelvin at the angle of observation. We rearrange, collapsing the beam profile term into the effective detector area and have an expression for $g_A g_B$:

$$g_A g_B = \frac{2S_{\pm Q, \mp U}}{A\delta\nu P_{\pm Q, \mp U}} \tag{10}$$

1.5 Scaling Lower Frequency Data to QUIET Frequencies

In order to compare polarized flux measurements in the literature to QUIET calibration signals, it is necessary to scale the data from the survey frequencies to slightly different QUIET frequencies. The spectral index, α of a source is the parameter giving how the intensity varies with frequency where $I \propto \nu^\alpha$. In order to show, however, how the temperature varies with frequency (in thermodynamic units for the CMB), we use the scaling relations:[7]

$$I_2 = I_1 \left(\frac{\nu_2}{\nu_1}\right)^\alpha \tag{11}$$

and then converting the intensity to temperature with the blackbody conversion from the previous section.

$$\begin{aligned} T &= \frac{I_{Jy}}{g_{RJ}\Omega_B} \\ &= \left(\frac{10^{26}c^2}{2k_B\nu_1^2\Omega_B}\right)\left(I_1\left(\frac{\nu_2}{\nu_1}\right)^\alpha\right) \end{aligned} \tag{12}$$

where ν_1 is the frequency at which the measurement was taken and ν_2 is the frequency we are scaling to.

2 Total Gain Uncertainty and Integration Time

For a point source whose polarized flux density we know in Janskys as F,

$$P = \frac{F\cos\left(\frac{\chi_i - (\Phi_d - \Phi_p)}{2}\right)}{g_{RJ}\Omega_B}$$

with which we may describe the expected diode signal $S_{\pm Q, \mp U}$ in terms of information from the literature.

$$S_{\pm Q, \mp U} = \frac{g_A g_B}{2} A\delta\nu\delta(\theta, \phi)B(\theta, \phi)P_{\pm Q, \mp U}$$

So, the total expression for the gain will be

$$g_i = g_A g_B = \frac{\pm 2 g_{RJ} \Omega_B S_{\pm Q, \mp U}}{\cos\left(\frac{\chi_i - (\Phi_d - \Phi_p)}{2}\right) F A_i \delta\nu [\delta(\theta,\phi) B(\theta,\phi)]} \tag{13}$$

This gain expression, for the practical purpose of determining uncertainty, can be collapsed into the two main contributors: the detector sensitivity and uncertainty of the known polarization as reported in the literature. [1]

$$\begin{aligned} g_i &\propto \frac{S}{T} \\ \Rightarrow \frac{\Delta g_i}{g_i} &= \sqrt{\left(\frac{\Delta S}{S}\right)^2 + \left(\frac{\Delta T}{T}\right)^2} \end{aligned} \tag{14}$$

Here,$\Delta T/T$ is the contribution from uncertainty in the literature. Even for well known sources this is on the order of 5%. $\Delta S/S$ is the S/N ratio achieved by the QUIET detectors. With Tau A and Cen A there is the potential that we can achieve S/N up to 170 per diode. Proposed target sensitivity of the module is described as [30]:

$$\Delta S = C_{CMB} \cdot \frac{T_{receiver} + T_{sky}}{\sqrt{\tau \cdot 2 \cdot 2 \cdot N}} \tag{15}$$

Array	C_{CMB}	T_{sky}	T_{rec}	τ (GHz)	N	$\Delta S_{N=1}\,(\mu K\sqrt{s})$
90 GHz	$\frac{1}{0.82}$	9K	45K	18 GHz	85	245
40 GHz	$\frac{1}{0.96}$	8K	19K	8 GHz	33	157
40 GHz	$\frac{1}{0.96}$	8K	19K	8 GHz	17	157
40 GHz	$\frac{1}{0.96}$	8K	35K	7.5 GHz	17	259

However, the actual noise levels are currenly reported as $0.6mK\sqrt{s}$ for the Q-Band 17 element array and $1mK\sqrt{s}$ for WBand, so those will be the values used for estimates in this document.

2.1 Scanning Efficiency

An efficient scanning pattern proposed by Akito Kusaka uses a stepwise staring motion for each horn. To avoid the $1/f$ knee, each horn may stare at the source for no more than 5 seconds. His scanning simulations of this tactic[2] give a 75% scanning efficiency.[13] So, 75% of the time that the telelscope is performing this procedure, one of the horns is staring at the source. With 17 horns, each horn can expect to spend 4.4% on source.

[1] c, k_B, detector frequency ν, and bandwidth, $\delta\nu$ are certainly known, so g_{RJ} contributes negligibly. A_i and $B(\theta,\phi)$ error bars will be found from beam shape studies, so we neglect them. Similarly, $\Phi_{p,d}$, the detector and polarization angles, can be neglected until data analysis. Source positions are considered known and the latitude of the telescope in Chajnantor is quite accurate (to the $(1/3600)^{th}$ of a degree).

[2] $da/dt = \frac{2.25^\circ}{s^3}$, $a < \frac{4.5^\circ}{s^2}$, $v < \frac{6.3^\circ}{s}$

3 Choosing Sources

By estimating the expected signal received by a QUIET module from a celestial source, and showing how observations of that signal can be expected to improve gain calibrations, we can determine what available sources will best suit our time constraints and calibration sensitivity requirements.

- The brightness of the source is inversely proportional to the square root of the observation time necessary for a given calibration sensitivity.
- Source area is directly proportional to observation time, and sources small enough to treat as point sources are much simpler analytically.
- The range of parallactic angles that the source traverses in the visible sky determines our capacity to isolate leakage terms and detector angle error.
- And finally, since the sun and moon are potentially overwhelming to the measurement, the time dependent proximity of the source to the sun and the moon are also factors in the scheduling of observations.

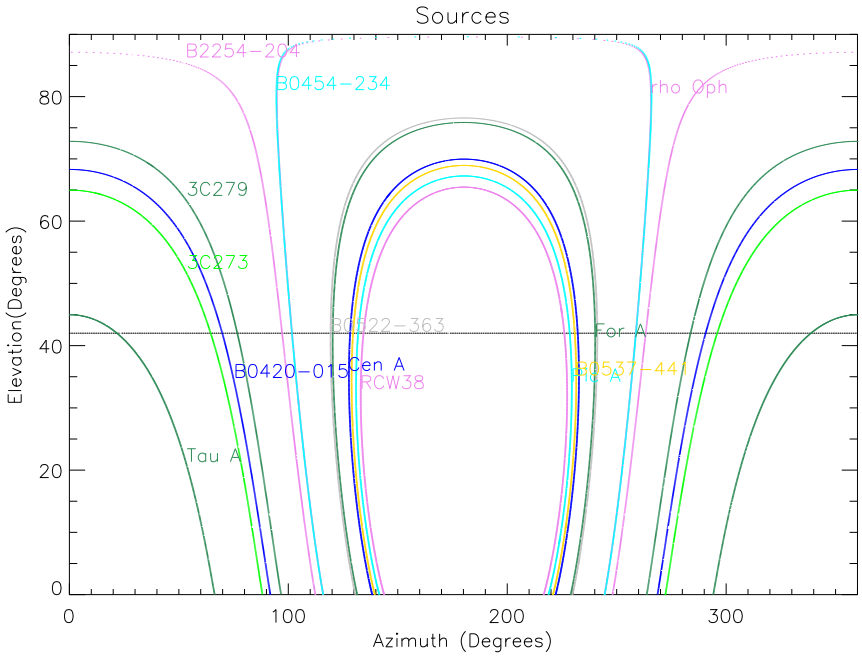

Figure 1: These are the Elevation-Azimuth paths of the potentially interesting known radio sources as observed from the telescope in Chajnantor. The telescope is able to see all Azimuth angles, but only Elevation angles above approximately 42°.

Thus, we seek compact, bright sources of well measured polarized flux and polarization, which cover broad ranges of parallactic angles and are usually far from both the sun and the moon. Unfortunately, in the southern hemisphere there are few well measured radio sources, and even fewer highly polarized pointlike radio sources that spend time above 42° telescope elevation, our lower pointing limit. Though many types of sources will be good candidates, most promising will be Taurus A and Centaurus A. To a lesser extent Pictor A, 3C273, 3C279, Jupiter, and (perhaps useful for limiting atmospheric effects) some small but bright southern blazars.

3.1 Seasonal Considerations

The sun and moon are incredibly bright. They overwhelm the signal of the sky around them so much that many CMB experiments make dramatic scheduling decisions based on their positions. Most experiments, for example, operate only at night. At the very least, QUIET may want to avoid scanning within 30° of the sun and moon. To investigate this, I accessed the IDL AstroLibrary and produced the following plots showing our sources of interest and their nearness to the sun and the moon over the course of the year.

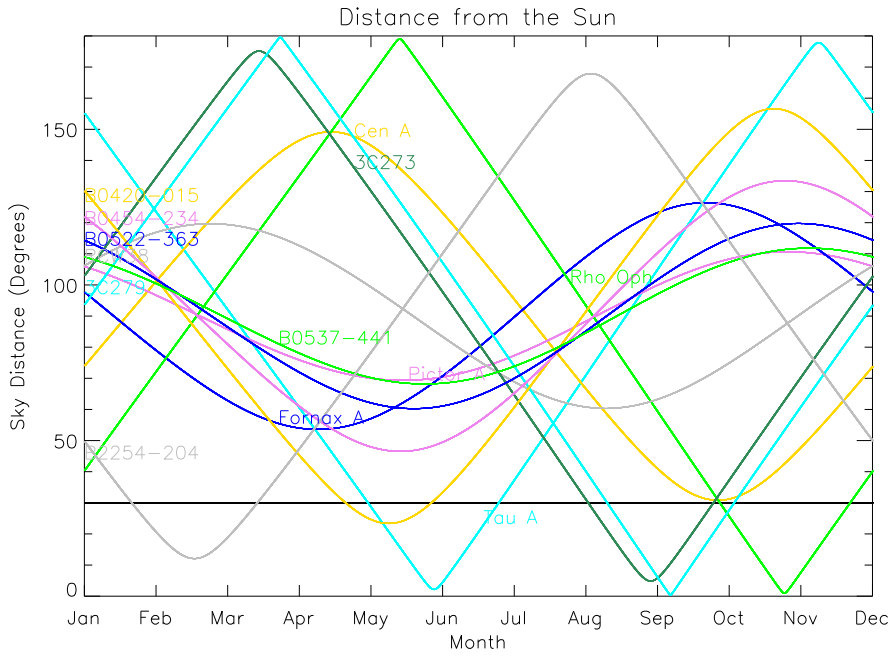

Figure 2: From the perspective of the telescope in Chajnantor over the course of 2008: This plot describes the distance in the sky(°) from the Sun of the potential calibration sources.

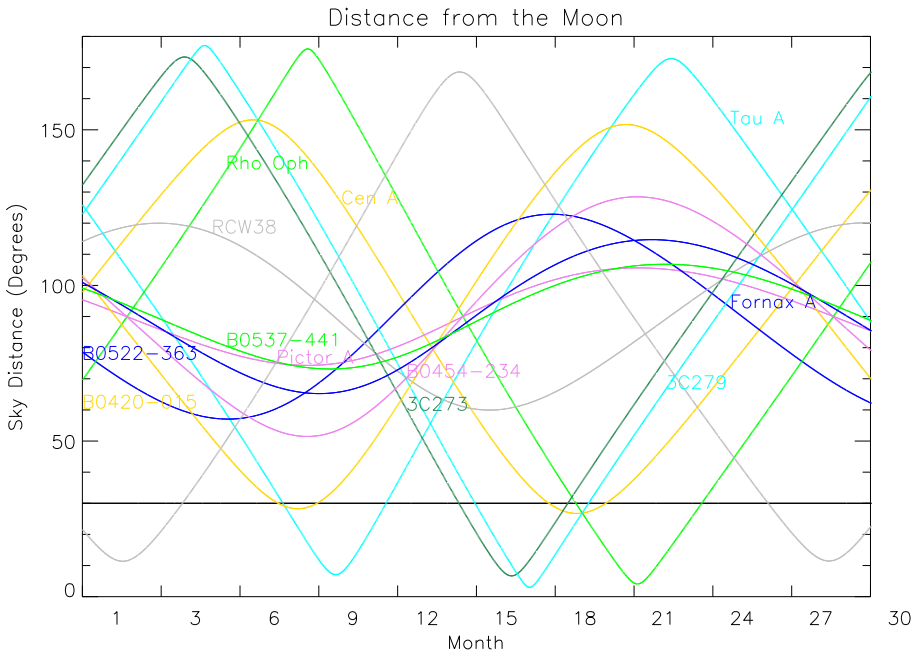

Figure 3: From the perspective of the telescope in Chajnantor over the course of one month: this plot describes the distance in the sky (°) from the Moon of the potential calibration sources.

3.2 Sources Near Scan Patches

The QUIET scan strategy will repeatedly scan four specific patches of the sky to observe E and B modes. To calibrate against sources near each of these patches will lend future data analysis a way to filter out possible atmospheric effects.

TauA and CenA are both well over 30° from any of the proposed patches, so they will not be useful in the filtration of atmospheric effects. For this purpose, other polarized point sources are considered. Many of these are blazars.

Blazars have a compact flat spectrum (where $\alpha \geq -0.5$ and $S(\nu) \propto \nu^{\alpha}$). So, strong blazars will have similar fluxes at frequency bands slightly lower than the Q and W bands we are interested in. This means that there are many surveys of these sources at frequencies that, though not in the Q and W bands, will nonetheless provide useful estimates of their predicted fluxes with very little uncertainty introduced in the spectral index frequency conversion. Some blazars near the patches with high polarized fluxes and large parallactic angle coverages are mentioned in the Appendix as well as a few other brightly polarized point sources that could be considered for this purpose.

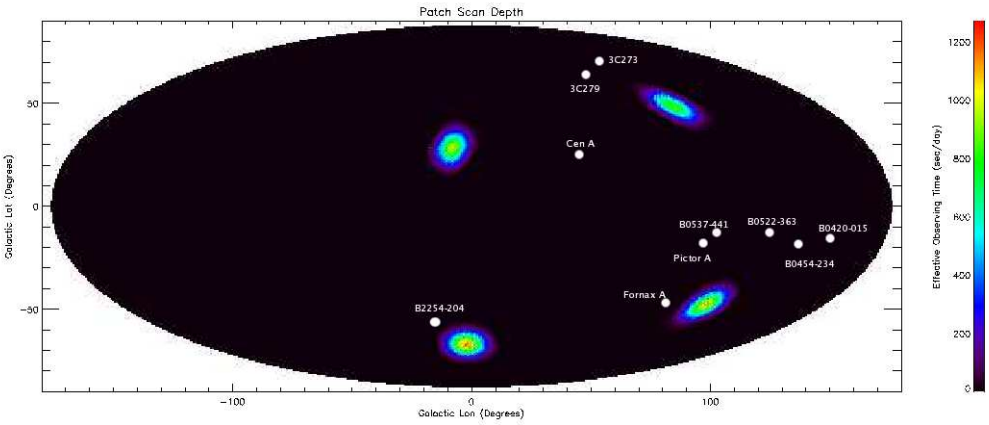

Figure 4: Locations of the four patches overlaid with locations of the potential sources near the patches. Though most of the blazars will not be suitably bright, they are the brightest point sources in close range of the patches. Background graphic of patches courtesy of Keith Vanderlinde, QUIET.[27]

Source	QBand (Jy)	WBand (Jy)	Pol. %	Pol. QBand (μK)	Pol. WBand (μK)
TauA	299 ± 6	229 ± 11	7.0 ± 0.3	$5,420.2 \pm 257$	4454.9 ± 287
CenA	34.8 ± 0.3	11.5 ± 0.4	13 ± 5	$1,171.6 \pm 46.2$	415.5 ± 286.7
PicA	4.4 ± 0.1	2.2 ± 0.4	29.6 ± 0.8	337.3 ± 12	181.0 ± 33
ForA	10.5 ± 2.5	0 ± 0	8.1 ± 2.2	220.3 ± 80	0.0
B0420	10.1 ± 0.2	6.4 ± 0.3	17 ± 1	444.7 ± 28	302.4 ± 23
B0454	2.6 ± 0.1	1.6 ± 0.4	27 ± 1	181.8 ± 10	120.1 ± 30
B0522	3.4 ± 0.1	2.6 ± 0.3	6.4 ± 0.5	56.4 ± 5	46.2 ± 6
B0537	5.7 ± 0.1	4.6 ± 0.4	3.4 ± 0.5	50.2 ± 7	43.5 ± 7
3C273	16.8 ± 0.1	10.5 ± 0.4	4.8 ± 0.8	208.8 ± 35	140.1 ± 24
3C279	18.2 ± 0.1	13.3 ± 0.4	3.8 ± 0.8	179.1 ± 38	140.5 ± 30
B2254	6.6 ± 0.1	5.2 ± 0.5	14.3 ± 0.63	244.4 ± 11	206.7 ± 22

Table 1: Flux Data from WMAP Point Source Catalog[31] and the associated Nonblind Catalog (Lopez-Caniego, 2007)[17]

With these temperatures we can apply the noise levels and scanning efficiency of the QUIET arrays to determine the S/N achievable with each source in a day.

4 Conclusion

The prime candidates for calibrating the QUIET QBand detectors will be Taurus A with which we can reach a S/N on some modules of ~ 170 (in 2.3

Source	Avail. hrs.	sec/day/module	Qband S/N
Tau A	2.3	365	172.7
CenA	7.1	1128	65.6
PicA	7.2	1144	19.0
ForA	7.2	1144	12.4
B0420	5.9	937	22.7
B0454	7.1	1128	10.2
B0522	7.2	1144	3.2
B0537	7.1	1128	2.8
3C273	5.6	889	10.4
3C279	6.2	985	9.4
B2254	6.9	1096	13.5
RCW38	6.9	1096	0
Jup	6.9	1096	0

Table 2: Flux Data from WMAP Point Source Catalog[31] and the associated Nonblind Catalog (Lopez-Caniego, 2007)[17] RCW38 and Jupiter are taken to be unpolarized, but since they are quite bright and available, they could be useful for pointing.

hours) and Centaurus A with which we can reach a S/N on all modules of ~ 65 (7 hours). The usefulness of Tau A is constrained by its limited arc in the sky. Some diodes higher on the array will be completely unable to view it without deck rotation. Furthermore, even with deck rotation it will be difficult to derive detector angle information from Tau A. Cen A suffers from neither of these issues, but calibration with a dimmer source like Cen A will much more time consuming. Other sources too still have merit, though less precision can be acheived with them in a realistic quantity of time. In the event that atmospheric concerns improve their attractiveness, these sources are discussed within the appendix.

Appendix

A Tau A

Tau A, also known as the Crab Nebula has a strongly emitting rotating neutron star pulsar at its heart. It is the most brightly polarized object in the sky, and so is a well known calibration resource for polarimetry experiments. With TauA it may be possible to achieve a S/N ratio of 170 in QBand. However, this will require deck rotation due to limited elevation in the southern sky.

Table 3: Tau A

RA	$05^h34^m31.97^s$	NED[19]
DEC	$22^d00^m52.1^s$	NED[19]
Gal. Longitude	184.557	NED[19]
Galactic Latitude	-5.784	NED[19]
41 GHz Total Flux (Jy)	299 ± 6	$WMAP$[31]
94 GHz Total Flux (Jy)	229 ± 11	$WMAP$[31]
α Spectral Index	-2.3	$WMAP$[31]
% Polarization (QBand)	$7.0 \pm 0.3\%$	$WMAP$[31]
% Polarization (WBand)	$7.6 \pm 2.0\%$	$WMAP$[31]
QBand Pol. Temp. (μK)	5420.2 ± 256	per module
WBand Pol. Temp. (μK)	4836.6 ± 1284	per module
Parallactic Angle Range	$\frac{-\pi}{3} \leq \chi \leq \frac{\pi}{3}$	[9]
Time above $42°(hrs.)$	2.268	[9]
Other Names	Messier 001 J0534+2200	Crab Nebula

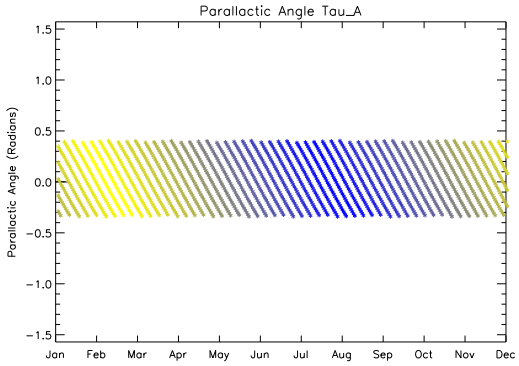

Figure 5: Range of parallactic angles reached by TauA over the course of a year above the telescope in Chajnantor. This includes the 42° lower cutoff in elevation. Blue indicates nighttime, yellow daytime.

B Centaurus A

Centaurus A is also known as NGC5128. It is a lenticular galaxy with giant radio lobes, one Northern Giant Lobe (NGL) and one Southern Giant Lobe (SGL). The NGL has a higher polarization than the SGL, and specificially within the NGL, there is a Northern Middle Lobe (NML) $20'$ north of the CenA nucleus that has a polarization fraction that reaches 40%. The highest polarized intensity will be 15% of the peak.

Table 4: Cen A

RA	$13^h25^m27.62^s$	NED[19]
DEC	$-43^d01^m8.8^s$	NED[19]
Galactic Longitude	309.516	NED
Galactic Latitude	+19.417	NED
41 GHz Total Flux (Jy)	34.8 ± 0.3	[17]
94 GHz Total Flux (Jy)	11.5 ± 0.4	[17]
α Spectral Index		WMAP[31]
% Polarization	$13 \pm 0.5\%$	Junkes [11]
QBand Pol. Temp. (μK)	$1,171.6 \pm 46.2$	per module
WBand Pol. Temp. (μK)	415.5 ± 286.7	per module
Parallactic Angle Range	$\frac{-4\pi}{3} \leq \chi \leq \frac{4\pi}{3}$	[9]
Time above $42°(hrs.)$	7.08	[9]
Other Names		NGC5128
		B1322-428
		J1325-4257

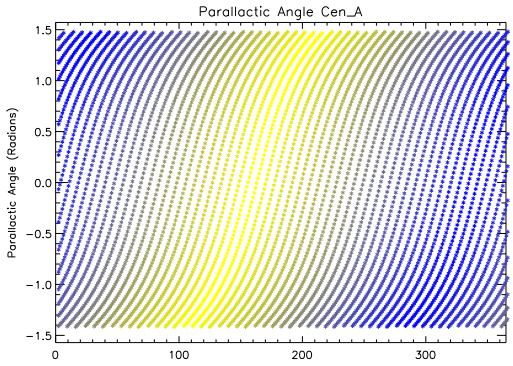

Figure 6: Range of parallactic angles reached by CenA over the course of a year above the telescope in Chajnantor. This includes the 42° lower cutoff in elevation. Blue indicates nighttime, yellow daytime.

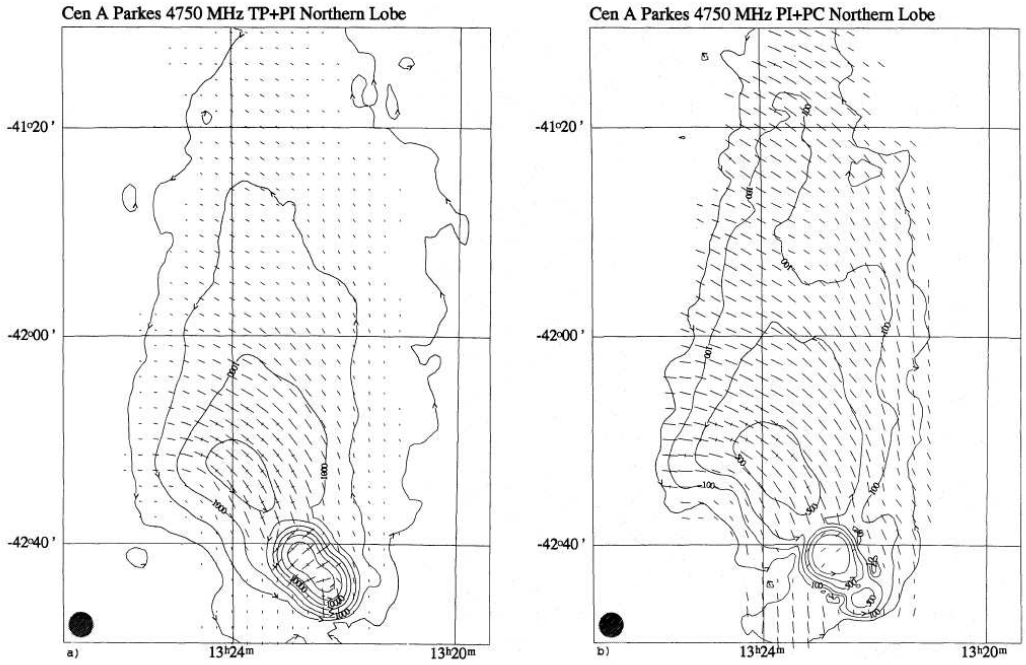

Fig. 2. a) A more detailed map of the total radio emission from the Northern Middle lobe (NML) of Cen A at λ6.3 cm. The rms noise level in the map is 20 mJy/b.a.. Contours indicate the intensity of the emission while E-vectors show the position angles of the polarized emission and their lengths its intensity (PI vectors starting at 50 mJy/b.a. with 500 mJy/b.a. or 1 t.u. as maximum value). **b)** A more detailed map of the polarized radio emission from the Northern Middle Lobe (NML) of Cen A at λ6.3 cm. The rms noise level in the map is 8 mJy/b.a.. Contour levels indicate the intensity of the polarized emission while E-vectors show the position angles of the polarized emission with their lengths showing percentage polarization (PC vectors starting at 10% with 40% or 1 t.u. as maximum value). Contour levels for both maps are shown in Table 3

Figure 7: $\lambda = 6.3$cm. $\Omega_B = 1.7 \times 10^{-}6$ steradians. [11]

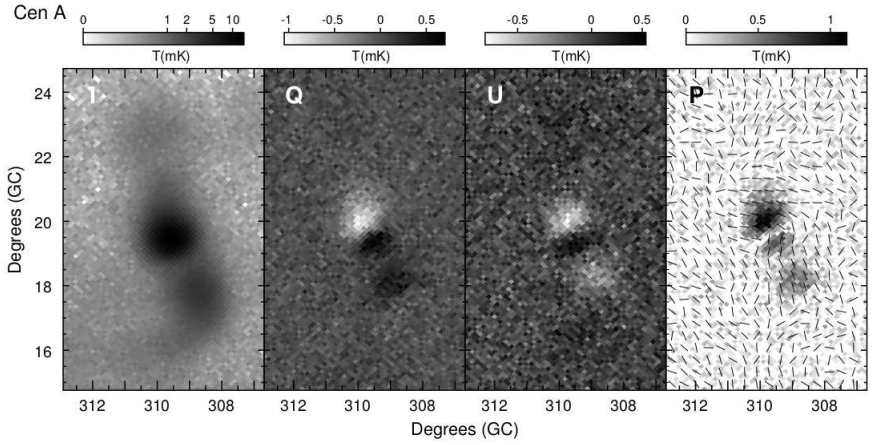

Figure 8: The WMAP data above shows the polarization profile of Centaurus A. This has been smoothed over each degree(°).[21]

C Pictor A

Pictor A is a galaxy with an unusually long jet. At the ends of this jet, to the east and west, are radio hotspots. The hotspot to the west is particularly highly polarized, with polarization fractions up to 63%[29], bright enough for special masking in the WMAP survey. The highest polarization intensity, however, is not at the point of highest polarization, so we use the lower limit on the polarization fraction in conjunction with the peak intensity[22][17].

Table 5: Pictor A

RA	$5^h19^m49.7^s$	NED[19]
DEC	$-45^d46^m44.5^s$	NED[19]
Gal. Longitude	251.597	NED[19]
Galactic Latitude	-34.6344	NED[19]
41 GHz Total Flux (Jy)	4.4 ± 0.1	$WMAP$[31]
94 GHz Total Flux (Jy)	2.2 ± 0.4	$WMAP$[31]
α Spectral Index	-0.7	$WMAP$[31]
% Polarization	$\geq 29.6 \pm 0.8\%$	VLA[22]
QBand Pol. Temp. (μK)	337.283 ± 11.9	per module
WBand Pol. Temp. (μK)	180.97 ± 33.3	per module
Size (arcmin)	$0.912' \times 0.724'$	NED[19]
Parallactic Angle Range	$\frac{-4\pi}{3} \leq \chi \leq \frac{4\pi}{3}$	[9]
Time above $42°(hrs.)$	7.08	[9]
Other Names	B0518-4549 WMAP J0519-4546 WMAP 150	

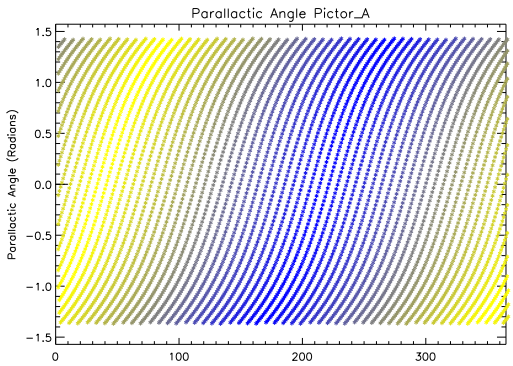

Figure 9: Range of parallactic angles reached by PicA over the course of a year above the telescope in Chajnantor. This includes the 42° lower cutoff in elevation. Blue indicates nighttime, yellow daytime.

D Fornax A

Fornax A is a massive lenticular galaxy in the Fornax cluster. Notably, it is visible to the Chajnantor site and above 42° in azimuth for 5 hours and 45 minutes a day and is very near the patch Keith calls patch 6. However, Fornax A has no significant reported flux in WBand whatsoever.

Table 6: Fornax A

RA	$3^h22^m41.7^s$	NED[19]
DEC	$-37^d12^m30^s$	NED[19]
Gal. Longitude	240.163	NED[19]
Galactic Latitude	-56.690	NED[19]
41 GHz Total Flux (Jy)	10.5 ± 2.5	$WMAP$[31]
94 GHz Total Flux (Jy)	0.0 ± 0.0	$WMAP$[31]
α Spectral Index	-0.8	$WMAP$[31]
% Polarization	$8.1 \pm 2.2\%$	$WMAP$[31]
QBand Pol. Temp. (μK)	220.3 ± 79.6	per module
WBand Pol. Temp. (μK)	0.0 ± 0.0	per module
Parallactic Angle Range	$\frac{-3\pi}{2} \leq \chi \leq \frac{3\pi}{2}$	[9]
Time above 42°($hrs.$)	7.224	[9]
Other Names	NGC1316 WMAP J0322-3711 WMAP 138	

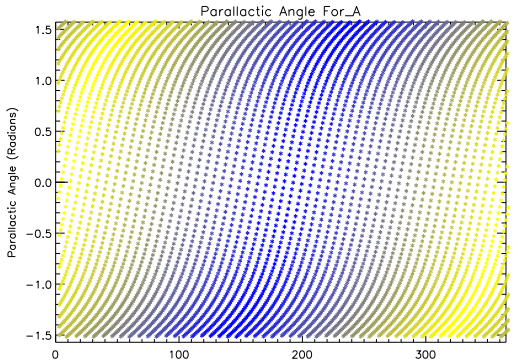

Figure 10: Range of parallactic angles reached by ForA over the course of a year above the telescope in Chajnantor. This includes the 42° lower cutoff in elevation. Blue indicates nighttime, yellow daytime.

E 3C273

3C273 is the brightest quasar in the sky. Specifically, it is a blazar so brightly polarized that WMAP specifically masked it out of their data. Notably, it is very near the patch Keith calls patch 4.

Table 7: 3C273

RA	$12^h29^m06.7^s$	NED[19]
DEC	$+02^d03^m09^s$	NED[19]
Galactic Longitude	289.951	NED
Galactic Latitude	64.359NED	
41 GHz Total Flux (Jy)	16.8 ± 0.1	$WMAP$[31]
94 GHz Total Flux (Jy)	10.5 ± 0.4	$WMAP$[31]
α Spectral Index	-0.3	$WMAP$[31]
% Polarization	$4.8 \pm 0.8\%$	$WMAP$[31]
QBand Pol. Temp. (μK)	208.83 ± 34.8	per module
WBand Pol. Temp. (μK)	140.06 ± 24.0	per module
Parallactic Angle Range	$-\pi \leq \chi \leq \pi$	
Size (arcmin)	$0.12' x 0.08'$	NED
Time above $42°(hrs.)$	5.6	[9]
Other Names		
	WMAP J1229+0203	[31]
	WMAP 170	[31]
	B1226+023	$PKSBlazar$

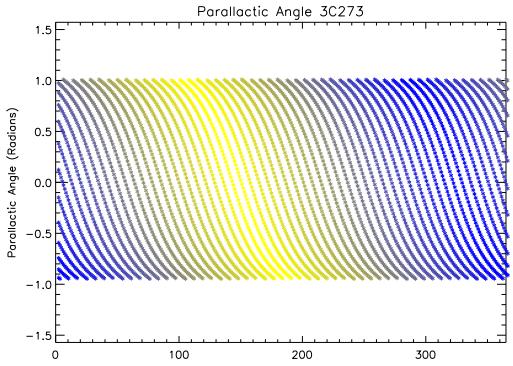

Figure 11: Range of parallactic angles reached by 3C273 over the course of a year above the telescope in Chajnantor. This includes the 42° lower cutoff in elevation. Blue indicates nighttime, yellow daytime.

F 3C279

3C279 is another superluminal radio quasar source. Particularly it is an OVV quasar with BL Lac (blazar) characteristics. 3C279 is highly variable, however, and this contributes to high uncertainty in the reported values for its fluxes and polarization fractions.

Table 8: 3C279

RA	$12^h56^m11.17^s$	NED[19]
DEC	$-05^d47^m21.5^s$	NED[19]
Galactic Longitude	305.104	NED[19]
Galactic Latitude	57.062	NED[19]
41 GHz Total Flux (Jy)	18.2 ± 0.1	$WMAP$[31]
94 GHz Total Flux (Jy)	13.3 ± 0.4	$WMAP$[31]
α Spectral Index	0.1	$WMAP$[31]
% Polarization	$3.8 \pm 0.8\%$	$WMAP$[31]
QBand Pol. Temp. (μK)	179.1 ± 37.7	per module
WBand Pol. Temp. (μK)	140.5 ± 29.9	per module
Parallactic Angle Range	$-\pi \leq \chi \leq \pi$	[9]
Time above $42°(hrs.)$	6.21	[9]
Other Names		
	B1253-055	
	J1256-0547	

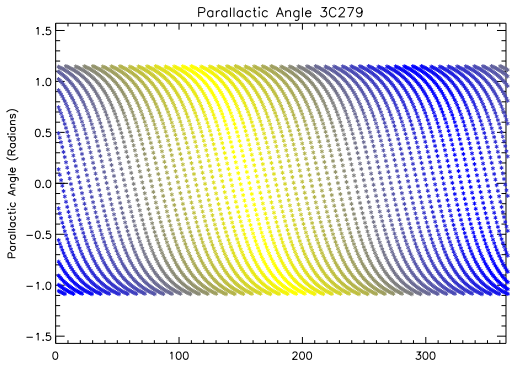

Figure 12: Range of parallactic angles reached by 3C279 over the course of a year above the telescope in Chajnantor. This includes the 42° lower cutoff in elevation. Blue indicates nighttime, yellow daytime.

G RCW 38

RCW38 is an ionized HII star forming region. While this source has been used as a calibrator for CMB experiments in the past, this was necessarily in conjunction with rotating metal gratings that essentially mimiced a 100% polarized source.

Table 9: RCW 38

RA	$08^h59^m47.2^s$	NED[19]
DEC	$-47^d31^m57^s$	NED[19]
Galactic Longitude	268.0339	NED[19]
Galactic Latitude	64.359	NED[19]
41 GHz Total Flux (Jy)	140	$WMAP$[21]
94 GHz Total Flux (Jy)	120 ± 0.5	$WMAP$[21]
α Spectral Index	0.115 ± 0.023	CBI[5]
% Polarization	$\leq 0.09\%$	$DASI$[16]
QBand pol. signal (μK)	0	per module
WBand pol. signal (μK)	0	per module
Parallactic Angle Range	$\frac{-4\pi}{3} \leq \chi \leq \frac{4\pi}{3}$	[9]
Time above $42°(hrs.)$	5.79	[9]
Other Names	$GAL268.0 - 01.1$	

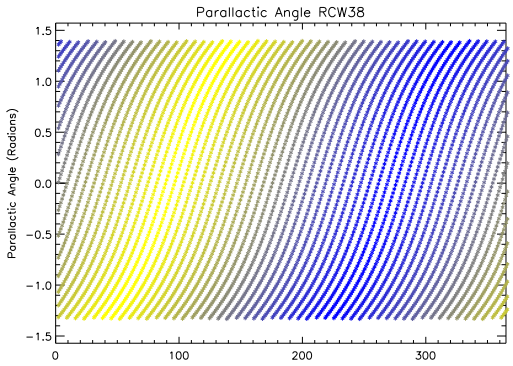

Figure 13: Range of parallactic angles reached by RCW38 over the course of a year above the telescope in Chajnantor. This includes the 42° lower cutoff in elevation. Blue indicates nighttime, yellow daytime. This is, of course, less useful, since there is no polarization axis for RCW38.

H B0454-234

B0454-234 is a brightly polarized blazar near patch 6.

Table 10: B0454-234

RA	$4^h57^m3.18^s$	NED[19]
DEC	$-23^d24^m52.0^s$	NED[19]
Galactic Longitude	223.710	NED
Galactic Latitude	-34.8968	NED
41 GHz Total Flux (Jy)	2.6 ± 0.1	WMAP[31]
94 GHz Total Flux (Jy)	1.6 ± 0.4	WMAP[31]
α Spectral Index	-0.1 ± 0.1	WMAP[31]
% Polarization	$27 \pm 1\%$	[26]
QBand Pol. Temp. (μK)	181.8 ± 9.7	per module
WBand Pol. Temp. (μK)	120.1 ± 30.3	per module
Time above $42°$($hrs.$)	7.068	[9]
Other Names		WMAP128

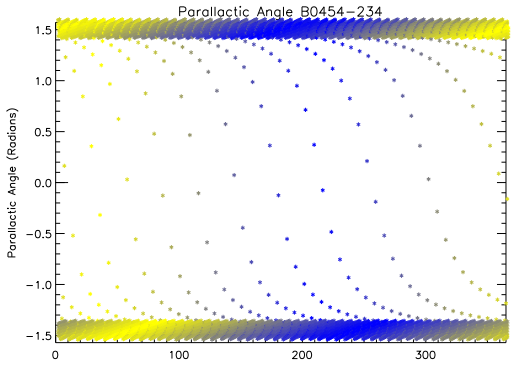

Figure 14: Range of parallactic angles reached by B0454-234 over the course of a year above the telescope in Chajnantor. This includes the 42° lower cutoff in elevation. Blue indicates nighttime, yellow daytime.

I B0537-441

B0537-441 is a high flux blazar. Due to its variability, WMAP did not report a significant polarization fraction, but its discovery in 1988 by Impey & Tapia was due to a polarization of 18.7% at 5GHz.

Table 11: B0537-441

RA	$05^h38^m43.5^s$	NED[19]
DEC	$-44^d05^m05^s$	NED[19]
Galactic Longitude	353.686	NED[19]
Galactic Latitude	+17.687	NED[19]
41 GHz Total Flux (Jy)	5.7 ± 0.1	$WMAP$[31]
94 GHz Total Flux (Jy)	4.6 ± 0.4	$WMAP$[31]
α Spectral Index	0.0 ± 0.05	$WMAP$[31]
% Polarization	$3.4 \pm 0.5\%$	$WMAP$[31]
QBand Pol. Temp. (μK)	50.19 ± 7.4	per module
WBand Pol. Temp. (μK)	43.47 ± 7.4	per module
Parallactic Angle Range	$-\pi \leq \chi \leq \pi$	Very Good
Variability	*high*	
Other Names	WMAP 148	

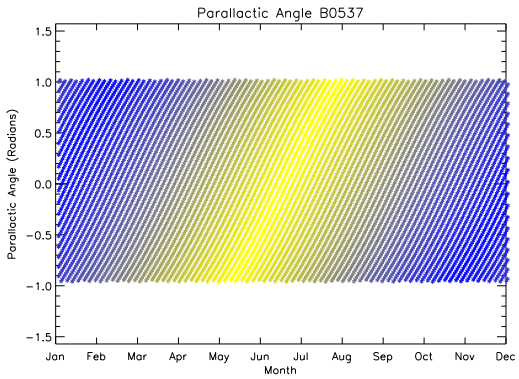

Figure 15: Range of parallactic angles reached by B0537-441 over the course of a year above the telescope in Chajnantor. This includes the 42° lower cutoff in elevation. Blue indicates nighttime, yellow daytime.

J B0420-015

B0420-015 is a medium flux blazar. However, it has been reported to have a very high polarization fraction. It is very near the patch Kieth calls patch 6.

Table 12: B0420-015

RA	$04^h23^m15.8^s$	NED[19]
DEC	$-01^d20^m33.07^s$	NED[19]
Galactic Longitude	195.29	NED[19]
Galactic Latitude	-33.1399	NED[19]
41 GHz Total Flux (Jy)	7.9 ± 0.1	$WMAP$[31]
94 GHz Total Flux (Jy)	4.9 ± 0.4	$WMAP$[31]
α Spectral Index	-0.1 ± 0.05	$WMAP$[31]
% Polarization	$17 \pm 1\%$	$WMAP$[26]
QBand Pol. Temp. (μK)	444.651 ± 27.6	per module
WBand Pol. Temp. (μK)	302.3 ± 22.7	per module
Parallactic Angle Range	$-\pi \leq \chi \leq \pi$	[9]
Variability	*high*	
Other Names		J0423-0120
		WMAP 110

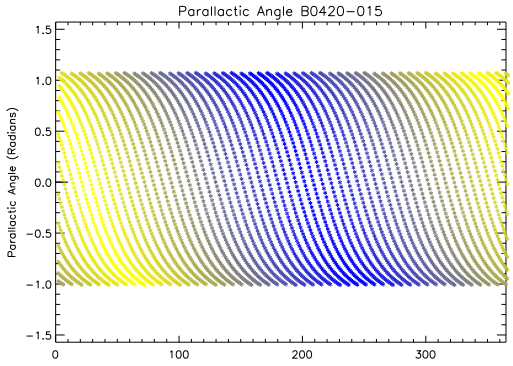

Figure 16: Range of parallactic angles reached by B0420-015 over the course of a year above the telescope in Chajnantor. This includes the 42° lower cutoff in elevation. Blue indicates nighttime, yellow daytime.

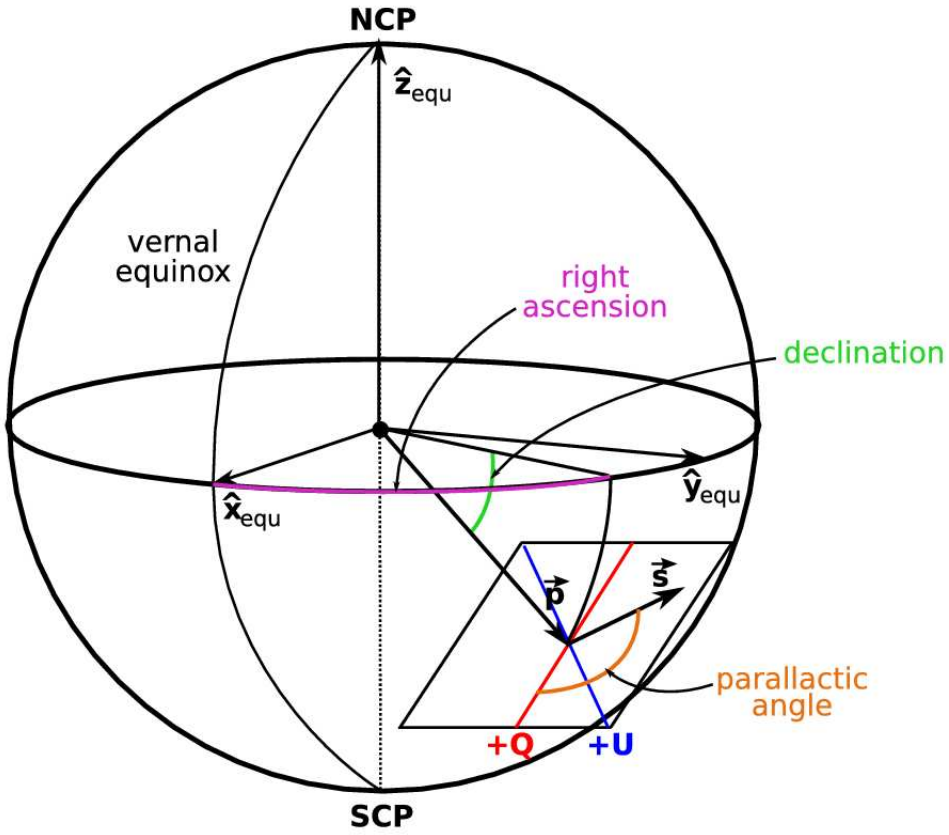

Figure 17: The definition of the basis vectors in the equatorial coordinate system. Image courtesy of Colin Bischoff. [2]

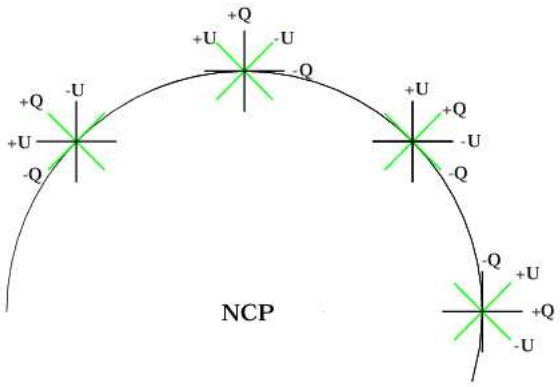

Figure 18: The definition of the Stokes parameters on the sky near the north celestial pole. [6]

References

[1] Alvarez, H. 2000. *The Radio Continuum Spectrum of Centaurus A's Large Scale Components*. A&A, 355, 863

[2] Bischoff, C. 2007. *Chicago Pointing and Coordinate Conventions*. QUIET internal document. (https://cmb.uchicago.edu/)

[3] Cotton, W.D. 1998. *Polarization Calibration of the MMA: Circular to Linear Feeds*. MMA Memo 208. (http://www.alma.nrao.edu/memos/html-memos/alma208/memo208.html#address)

[4] Dickinson, C. 2005. *Large Scale (1.4m) QUIET Beam Patterns v1.2*. QUIET internal document (QUIETbeamsv3.pdf).

[5] Dickinson, C., Davies, R.D., Bronfman, L., Casassus, S., Davis,R.J., Pearson, T.J., Readhead, A.C.S., Wilkinson, P.N. 2007. *CBI limits on 31 GHz excess emission in southern H ii regions.* Monthly Notices of the Royal Astronomical Society 379 (1), 297307.

[6] Hedman, M.M. 2002. *The Princeton IQU Experiment and Constraints on the Polarization of the Cosmic Microwave Background at 90 GHz*. Ph.D. thesis, Princeton University.

[7] Hedman, M.M. 2003. *Polarimetry Channel Calibration*. CAPMAP internal document (cal_0903.ps).

[8] Hu, W., & White, M. 1997. *A CMB Polarization Primer*. New Astronomy, 2, 323.

[9] IDL Astronomy library.

[10] Jarosik, N., et.al., 2007. *Three-Year Wilkinson Microwave Anisotropy Probe (WMAP) Observations: Beam Profiles, Data Processing, Radiometer Characterization and Systematic Error Limits*, ApJS, 170, 263.

[11] Junkes, N., & Haynes, R.F. 1991. *The Large-scale Radio Structure of Centaurus A*

[12] Kusaka, A., *Possible Improvement in Scanning*. QUIET internal document. https://cmb.uchicago.edu/project/images/4/48/Simulation_scan_improvement-v2.pdf. 2007.

[13] Kusaka, A., *Calibration Presentation for Collaboration Meeting*. May 2008. https://cmb.uchicago.edu/project/index.php/2008_May_15/16_Collaboration_Meeting_%40_CIT.

[14] Lazendic, J.S., Dickel, J.R., Haynes, R.F., Jones, P.A., & White, G.L. 2000. ApJ 540,808

[15] Limon, M. et. al. 2008. *Wilkinson Microwave Anisotropy Probe (WMAP) Five-Year Explanatory Supplement* (Greenbelt, MD: NASA/GSFC). http://lambda.gsfc.nasa.gov.

[16] Leitch,E.M., Kovac,J.M., Pryke,C., Reddall,C., Sandberg,E.S., Dragovan,M., Carlstrom,J.E., Halverso,N.W., Holzapfel, W.L. 2002. *Measuring Polarization with DASI* Nature 420, 763-771.

[17] Lopez-Caniego,M., Gonzalez-Nuevo,J., Herranz,D. May 2007. ApJ Suppl. Series, 170:108-125.

[18] McMahon, J. 2006. *The 2004-2005 CAPMAP Instrument and CMB Polarization Data*. Ph.D. thesis, Princeton University. Chapter 4.

[19] NASA/IPAC Extragalactic Database (NED). JPL , Cal.Inst.Tech., http://nedwww.ipac.caltech.edu/. 2008.

[20] Nixon, G. 2006. *Tau A*. CAPMAP internal document (TauA Gains 2005.pdf).

[21] L. Page, et.al., 2007. *Three-Year Wilkinson Microwave Anisotropy Probe (WMAP) Observations: Polarization Analysis*, ApJS, 170, 335.

[22] Perley,R.A., Roser,H.J., Meisenheimer,K. 1997. *The Radio Galaxy Pictor A - A Study with the VLA* A&A 328, 12-32.

[23] Roser,H.J., Meisenheimer, K. 1987. *A Bright Optical Synchotron Counterpart of the Wester Hot Spot in Pictor A* ApJ, 314, 70-75.

[24] Shen, Z.Q. et. al. 1998. *A 5GHz Southern Hemisphere VLBI Survey of Compact Radio Sources - II*. Arxiv preprint astro-ph/9803104.

[25] Sugarbaker, A. 2007. *1/f Noise in QUIET Polarimeters*. QUIET internal document (https://cmb.uchicago.edu/project/images/6/64/Sugarbaker_spr_thesis.pdf).

[26] Torniainen,I., Tornikoski,M., Tersranta,H, Aller,M.F., Aller,H.D. *Long term variability of gigahertz-peaked spectrum sources and candidates*A&A 435, 839-856.

[27] Vanderlinde, K., Winstein, B., Smith, K. *Notes on QUIET Scanning*. QUIET Internal Document. https://cmb.uchicago.edu/project/images/8/82/Scanning.pdf. 2006.

[28] Winstein, B. et al. *QUIET Collaboration*. http://quiet.uchicago.edu. Based on NSF proposal, 2004.

[29] Wagner,S.J., Bicknell,G., Szeifert,T., 2001. *Polarization observations of the hot-spot Pictor A West: shocks in backflows?* ASP Conference Proceedings Vol. 250, p.259.

[30] Winstein, B. *Module Acceptance document.* https://cmb.uchicago.edu/project/images/2/2f/Module_acceptance.pdf.

[31] *Three-Year Wilkinson Microwave Anisotropy Probe (WMAP) Derived Foreground Products: Point Source Catalog*, (http://lambda.gsfc.nasa.gov/product/map/dr2/ptsrc_catalog_info.cfm).

[32] Xephem Version 3.7.2. Downey, E.C. 2006.

[33] Finally, I would very much like to thank the QUIET collaboration. Thanks first to Bruce Winstein for support, guidance, and patience throughout all of my undergraduate years. Thanks of course to Colin Bischoff, Dan Kapner and Ali Brizius for their constant help and bright answers to my innumerable questions over that time, and finally to Dorothea Samtleben, Glenn Nixon, and especially Akito Kusaka for their assistance in the completion of this document.